A Non-standard Anisotropic Diffusion for Speckle Noise Removal

Hyeona LIM
Department of Mathematics and Statistics, Mississippi State University
Mississippi State, MS 39762 USA

and

Thomas Neil WILLIAMS
Center for Advanced Vehicular Systems, Mississippi State University, Box 5405
Mississippi State, MS 39762, USA

ABSTRACT

The main objective of this article is to develop a non-standard partial differential equation-based anisotropic diffusion model for efficient edge-preserving denoising for speckle noised images. The standard total variation (TV)-based energy functional is not based on the multiplicative-ness of speckle noise which is inappropriate for a speckle noise removal. Moreover, TV-based models can easily lose fine structures and produce non-physical dissipation during the noise removal process. The principal feature in this article is an introduction of a new coefficient for the non-linear diffusion term of the Euler-Lagrange equation corresponding to the minimization of the energy functional. Combination of a new model with a texture-free residual parametrization enables us to overcome the drawback arising from use of the standard TV-based model. The numerical results indicate the effectiveness and robustness of the new model.

Keywords: Anisotropic diffusion, speckle noise, fine structures, denoising, total variation (TV) model, nonphysical dissipation, texture-free residual parametrization.

1. INTRODUCTION

Images in our daily lives occur in many forms such as digital or analog pictures, scanned documents, satellite pictures, and scanning electron microscopes (SEM) images. Not only can images from the visible portion of the electromagnetic spectrum be detected, but sensors can detect and produce images from infrared and ultraviolet light, X-rays, γ-rays, microwaves, and radio waves, as well. Signals other than electromagnetic radiation can be also imaged [16].

Many of these image applications are produced in the following processing steps: An imaging system, such as an objective lens or a collimator, converts a three-dimensional real-world scene to a two-dimensional image, and subsequently a sensor system, such as a digital camera or a scanner, converts the image into an electrical signal. The image generated by a picture digitization generally produces errors due to a mechanical imperfection or physics of picture acquisition. Especially, the noise inherent in the electronics of the photo-receptors adds a noise.

Many applications in modern age rely on good quality of images and therefore, various techniques of image restoration that improve the quality of images take on a very important role.

Mathematically based image restoration techniques have emerged to answer fundamental questions, such as a higher level of efficiency and reliability, arising in the field of image processing. For the last decade or so, partial differential equations (PDE)-based models have been developed for various physical applications in image restoration [1, 2, 4, 8, 12, 13, 14, 15, 17].

Image distortion is usually caused by a space invariant blur accompanied by an additive Gaussian noise. Thus the observed (distorted) image f can be represented by the form

$$f = K * u + n, \tag{1}$$

where $*$ denotes convolution, n represents the Gaussian noise, and u is the desired image to find. Here K is a blurring operator, where the integral over the domain is unity, that is,

$$\int_\Omega K \, d\mathbf{x} = 1, \quad K \geq 0. \tag{2}$$

In this article we assume that $K = I$, the identity operator since our main concern is to remove noise. A common variational technique for denoising is to minimize a functional given as

$$\min_u F_p(u), \qquad F_p(u) = \int_\Omega |\nabla u|^p \, d\mathbf{x} + \frac{\lambda}{2} \|f - u\|_2^2, \tag{3}$$

where $\lambda \geq 0$ is a Lagrange multiplier and $\|\cdot\|_2$ denotes the L^2-norm.

The corresponding *Euler-Lagrange equation* for the minimization of energy functional Eq. (3) is

$$-p \, \nabla \cdot \Big(\frac{\nabla u}{|\nabla u|^{2-p}} \Big) - \lambda \, (f - u) = 0. \tag{4}$$

For a dynamic iterative numerical simulation of Eq. (4), we introduce energy descent direction by an artificial time t and we obtain the following evolutionary parabolic-type nonlinear equation:

$$\frac{\partial u}{\partial t} - \nabla \cdot \Big(\frac{\nabla u}{|\nabla u|^{2-p}} \Big) \;=\; \frac{\lambda}{p}(f-u). \tag{5}$$

The above equation can be numerically solved iteratively with no-flux boundary condition and with the given noised image f as an initial data. Note that when $1 \le p \le 2$, the model Eq. (5) can easily lose fine structures due to nonphysical dissipation. In order to prevent the denominator $|\nabla u|$ in Eq. (5) approaching zero, it must be regularized as

$$|\nabla u| \;\approx\; |\nabla^{\varepsilon} u| \;:=\; (u_x^2 + u_y^2 + \varepsilon^2)^{1/2} \tag{6}$$

for some $\varepsilon > 0$ small. Such a regularization can be a significant source of nonphysical dissipation [9].

When $p = 1$, the model Eq. (5) becomes the *total variation* (TV) model [15]. Notice that $|\nabla u|^{-1}$ in the diffusion term $\nabla \cdot \Big(\frac{\nabla u}{|\nabla u|} \Big)$ of the TV model is huge on the flat region and small near edges. Such a different speed of diffusion in different regions is a desirable property for an edge-preserving noise removal. However, it has been practically shown that the TV model tends to produce locally constant images, which is called the staircasing effect. In order to prevent this, Marquina and Osher [12] introduced the *improved TV* (ITV) model

$$\frac{\partial u}{\partial t} - |\nabla u| \, \nabla \cdot \Big(\frac{\nabla u}{|\nabla u|} \Big) \;=\; \lambda \, |\nabla u| \, (f-u) \tag{7}$$

by scaling the TV model by a factor of $|\nabla u|$. It has been however recently analyzed in [3] that ITV model can hardly reduce nonphysical dissipation.

In order to prevent such nonphysical dissipation, Kim and Lim have introduced in their recent paper [9] the following non-convex model:

$$\frac{\partial u}{\partial t} - |\nabla u|^{1+\omega} \nabla \cdot \Big(\frac{\nabla u}{|\nabla u|^{1+\omega}} \Big) \;=\; \beta \, (f-u), \quad \omega \in (0,1), \tag{8}$$

where $\beta = \beta(\mathbf{x}, t) \ge 0$. It has been numerically verified in [9] that the stable algorithm associated with the above non-convex model combined with texture-free residual (TFR) parametrization can reduce nonphysical dissipation. The model is also very effective in simultaneous denoising and edge enhancement. However, the model is mathematically unstable since ω is between 0 and 1.

The above TV-based models are based on the assumption that the image distortion is based on additive Gaussian noise (See Eq. (1)). Thus they are not appropriate for images having speckle noise since speckle noise is normally multiplicative, not additive. In this article, we develop a mathematically stable model based on the TV minimization which can efficiently remove speckle noise while reducing nonphysical dissipation of the model. The principal technique is based on the introduction of a new coefficient for the non-linear diffusion term to provide an efficient process of speckle noise removal.

An outline of the paper is as follows. In the next section, we develop a new model based on the TV minimization. In Section 3, we discuss about the numerical procedure for our new model and briefly review TFR parametrization. Section 4 contains numerical results to show the effectiveness of the new model. The last section includes conclusions.

2. A NEW ANISOTROPIC DIFFUSION MODEL

The speckle noise which is mostly present in ultrasound images, synthetic aperture radar (SAR) images, or acoustic images is often assumed to be multiplicative and experimental results show that it can be modeled as [10, 11]

$$f = u + \sqrt{u} n, \tag{9}$$

where u is the desired image to find, n is Gaussian noise, and f denotes the observed image. Then from energy minimization of the corresponding functional, the following TV-based model can be derived:

$$\frac{\partial u}{\partial t} - \frac{u^2}{f+u} |\nabla u| \, \nabla \cdot \Big(\frac{\nabla u}{|\nabla u|} \Big) \;=\; \lambda \, |\nabla u| \, (f-u). \tag{10}$$

Here note that the coefficient of the diffusion term $|\nabla u| \, \nabla \cdot \Big(\frac{\nabla u}{|\nabla u|} \Big)$ is $\frac{u^2}{f+u}$ and $\frac{u^2}{f+u} \approx u/2$ assuming that $f \approx u$. Therefore, the model Eq. (10) can be interpreted as a variant of the ITV model with a constant multiple of u multiplied by the diffusion term. This coefficient makes the diffusion faster in the lighter region (where the image values are high) and slower in the darker region (where the image values are low). Diffusion is associated with the noise removal. That is, noise is removed or reduced from the diffusion process due to the second term in Eq. (10). Thus the model Eq. (10) is unrealistic and ineffective in practice since noise can be present anywhere in the image, not only in the lighter region. For this reason, we propose the following form of a noise model:

$$f = u + \big(\sqrt{u - u_s} \big) \, n, \tag{11}$$

where f, u, n are the same as before and u_s denotes smoothed version of the noised image f. From the associated minimization of the functional, we derive a new non-standard anisotropic diffusion (NSAD) model:

$$\frac{\partial u}{\partial t} - C|u - u_s|^{\alpha} |\nabla u| \, \nabla \cdot \Big(\frac{\nabla u}{|\nabla u|} \Big) \;=\; \lambda \, |\nabla u| \, (f-u), \tag{12}$$

where C is a constant which will be numerically found. Since the values of u and f are scaled to between 0 and 1, we need a proper constant C. For stability reasons, C can not be chosen to be too large. From the numerical experiments, the best choice of α is known to be in between $1/2$ and 2. Our new model Eq. (12) has the following desirable properties:

- On the regions where noise is present, $|u - u_s|$ is relatively big. Therefore with an appropriate multiple of the constant C, diffusion (the second term of the model Eq. (12)) is big enough to reduce the noise efficiently.

- On the regions where noise is not present, $|u - u_s|$ is small. Thus diffusion is relatively slower which can prevent any nonphysical dissipation due to excessive diffusion.

In the next section, we discuss a numerical procedure for our new model. For more efficient edge-preserving noise removal, we adopt TFR parametrization which was developed in [9] for our new model Eq. (12) and briefly review the procedure in the second subsection.

3. THE NUMERICAL PROCEDURE

The linearized θ-method

Denote the timestep size by Δt. Set $t^n = n\Delta t$ and $u^n = u(\cdot, t^n)$ for $n \geq 0$. Then, Eq. (12) can be linearized by evaluating the nonlinear parts from the previous time level. Consider the linearized θ-method for Eq. (12) of the form:

$$\begin{aligned} & \frac{u^n - u^{n-1}}{\Delta t} + (\mathcal{A}^{n-1} + \beta^n I)\,[\theta u^n + (1-\theta)u^{n-1}] \\ = \quad & \beta^n f, \quad 0 \leq \theta \leq 1, \end{aligned} \tag{13}$$

where $\mathcal{A}^{n-1}$ is a spatial approximation of a linearized diffusion operator, i.e.,

$$\begin{aligned} & \mathcal{A}^{n-1}u^m \approx -C|u^{n-1} - u_s|^\alpha |\nabla^\varepsilon u^{n-1}| \nabla \cdot \Big(\frac{\nabla u^m}{|\nabla^\varepsilon u^{n-1}|}\Big), \\ & m = n-1, n. \end{aligned} \tag{14}$$

Here $|\nabla^\varepsilon u| := (u_x^2 + u_y^2 + \varepsilon^2)^{1/2}$ is a regularization of $|\nabla u|$ to prevent the denominator from approaching zero. β^n is chosen as

$$\beta^n := \lambda^n |\nabla^\varepsilon u^n|. \tag{15}$$

To improve efficiency of the computation of Eq. (13), we set $\mathcal{A}^{n-1} = \mathcal{A}_1^{n-1} + \mathcal{A}_2^{n-1}$, where

$$\begin{aligned} & \mathcal{A}_\ell^{n-1}u^m \approx -C|u^{n-1} - u_s|^\alpha |\nabla^\varepsilon u^{n-1}|\, \partial_{x_\ell}\Big(\frac{\partial_{x_\ell} u^m}{|\nabla^\varepsilon u^{n-1}|}\Big), \\ & \ell = 1, 2. \end{aligned} \tag{16}$$

Here $(\partial_{x_1}, \partial_{x_2})^T$ is a spatial finite difference approximation of ∇ which will be constructed later in this section. Using these separable matrix operators $\mathcal{A}_1^{n-1}$ and $\mathcal{A}_2^{n-1}$ in Eq. (16), the *alternating direction implicit* (ADI) method [5, 6], which is a perturbation of Eq. (13) with a splitting error of $\mathcal{O}(\Delta t^2)$, has been employed.

Now, we construct the matrix $\mathcal{A}_1^{n-1}$. Let $\mathcal{D}\, u_{i-1/2,j}^{n-1}$ be a finite difference approximation of $|\nabla u^{n-1}|$ evaluated at $\mathbf{x}_{i-1/2,j}$, the mid point of $\mathbf{x}_{i-1,j}$ and $\mathbf{x}_{i,j}$. Define

$$d_{ij,W}^{n-1} = [(\mathcal{D}\, u_{i-1/2,j}^{n-1})^2 + \varepsilon^2]^{1/2}, \quad d_{ij,E}^{n-1} = d_{i+1,j,W}^{n-1}. \tag{17}$$

Then the differential operators in Eq. (16) can be approximated as

$$\begin{aligned} -\partial_{x_1}\Big(\frac{\partial_{x_1} u^m}{|\nabla^\varepsilon u^{n-1}|}\Big) \quad &\approx \quad -\frac{1}{d_{ij,W}^{n-1}} u_{i-1,j}^m \\ & \quad + \Big(\frac{1}{d_{ij,W}^{n-1}} + \frac{1}{d_{ij,E}^{n-1}}\Big) u_{i,j}^m \\ & \quad - \frac{1}{d_{ij,E}^{n-1}} u_{i+1,j}^m, \\ |\nabla^\varepsilon u^{n-1}| \quad &\approx \quad 2\frac{d_{ij,W}^{n-1} \cdot d_{ij,E}^{n-1}}{d_{ij,W}^{n-1} + d_{ij,E}^{n-1}}. \end{aligned} \tag{18}$$

By combining the right sides of equations in Eq. (18), we can obtain the three consecutive non-zero elements of the matrix $\mathcal{A}_1^{n-1}$ corresponding to the pixel $\mathbf{x}_{ij}$:

$$[\mathcal{A}_1^{n-1}]_{ij} = C|u_{ij}^{n-1} - u_{s,ij}|^\alpha (-a_{ij,W}^{n-1},\, 2,\, -a_{ij,E}^{n-1}), \tag{19}$$

where

$$a_{ij,W}^{n-1} = \frac{2\, d_{ij,E}^{n-1}}{d_{ij,W}^{n-1} + d_{ij,E}^{n-1}}, \quad a_{ij,E}^{n-1} = \frac{2\, d_{ij,W}^{n-1}}{d_{ij,W}^{n-1} + d_{ij,E}^{n-1}}. \tag{20}$$

Similarly, $\mathcal{A}_2^{n-1}$ corresponding to the pixel $\mathbf{x}_{ij}$ can be obtained:

$$[\mathcal{A}_2^{n-1}]_{ij} = C|u_{ij}^{n-1} - u_{s,ij}|^\alpha (-a_{ij,S}^{n-1},\, 2,\, -a_{ij,N}^{n-1}), \tag{21}$$

where

$$a_{ij,S}^{n-1} = \frac{2\, d_{ij,N}^{n-1}}{d_{ij,S}^{n-1} + d_{ij,N}^{n-1}}, \quad a_{ij,N}^{n-1} = \frac{2\, d_{ij,S}^{n-1}}{d_{ij,S}^{n-1} + d_{ij,N}^{n-1}}. \tag{22}$$

Combining these approximations with the same ADI procedure in [9, §3.2], our linearized θ-method Eq. (13) satisfies the following stability theorem.

Theorem 3.1. *Define* $\beta_0 = \min_{i,j,n} \beta_{ij}^n$ *and* $\beta_1 = \max_{i,j,n} \beta_{ij}^n$. *Denote* $b^* := C \max_{i,j,n} |u_{ij}^{n-1} - u_{s,ij}|^\alpha$. *Let*

$$(4b^* + \beta_1)\,(1-\theta)\Delta t \leq 1. \tag{23}$$

Then the θ-method Eq. (13) *associated with the numerical scheme in Eqs.* (17)-(22) *is stable and holds the maximum principle.*

Proof. It is sufficient to show the following inequality:

$$\min_{i,j} f_{ij} \;\leq\; u_{ij}^n \;\leq\; \|f\|_\infty, \quad n \geq 0, \tag{24}$$

which implies the maximum principle and stability. Let $M_{ij} := C|u_{ij}^{n-1} - u_{s,ij}|^\alpha$. Then the Eq. (13) at a point

$\mathbf{x}_{ij}$ can be written as

$$\begin{aligned}
& [1 + (4M_{ij} + \beta_{ij}^n)\theta\Delta t]\, u_{ij}^n \\
= \;& \theta\Delta t M_{ij}\, [a_{ij,W}^{n-1}\, u_{i-1,j}^n + a_{ij,E}^{n-1}\, u_{i+1,j}^n \\
& + a_{ij,S}^{n-1}\, u_{i,j-1}^n + a_{ij,N}^{n-1}\, u_{i,j+1}^n] \\
& + (1-\theta)\Delta t M_{ij}\, [a_{ij,W}^{n-1}\, u_{i-1,j}^{n-1} + a_{ij,E}^{n-1}\, u_{i+1,j}^{n-1} \\
& + a_{ij,S}^{n-1}\, u_{i,j-1}^{n-1} + a_{ij,N}^{n-1}\, u_{i,j+1}^{n-1}] \\
& + [1 - (4M_{ij} + \beta_{ij}^n)(1-\theta)\Delta t]\, u_{ij}^{n-1} \\
& + \Delta t \beta_{ij}^n\, f_{ij}. \qquad (25)
\end{aligned}$$

Let u_{ij}^n be a local minimum. Note that u_{ij}^n is smaller than or equal to the nine neighboring values:

$$\begin{aligned}
& u_{i-1,j}^n, u_{i+1,j}^n, u_{i,j-1}^n, u_{i,j+1}^n, \\
& u_{i-1,j}^{n-1}, u_{i+1,j}^{n-1}, u_{i,j-1}^{n-1}.u_{i,j+1}^{n-1}, u_{ij}^{n-1}. \qquad (26)
\end{aligned}$$

Notice also that the following identity holds:

$$a_{ij,W}^m + a_{ij,E}^m + a_{ij,S}^m + a_{ij,N}^m = 4, \quad m = n-1,\, n. \quad (27)$$

Using the conditions Eqs. (26), (27), and the inequality given in Eq. (23), one can conclude that each of coefficients in the right side of Eq. (25) is nonnegative and therefore the Eq. (25) becomes

$$\begin{aligned}
& [1 + (4M_{ij} + \beta_{ij}^n)\theta\Delta t]\, u_{ij}^n \\
\geq \;& [1 + (4M_{ij} + \beta_{ij}^n)\theta\Delta t]\, u_{ij}^n - \Delta t \beta_{ij}^n\, (u_{ij}^n - f_{ij}). \qquad (28)
\end{aligned}$$

Thus the second term $\Delta t \beta_{ij}^n\, (u_{ij}^n - f_{ij})$ in the right side of inequality Eq. (28) must be positive. This implies that

$$f_{ij} \leq u_{ij}^n.$$

The inequality holds for all local minima, which proves the first inequality in Eq. (24). The same argument can be applied for local maxima to verify the other inequality. This completes the proof. □

The TFR Parametrization

In literature, the parameter λ has been chosen constant for most cases; the resulting model either smears out some important portions more excessively than desired or leaves a certain amount of noise in the restored image. In order to overcome the difficulty, the parameter must become larger wherever dissipation is excessive, while being small elsewhere. In the following, we will consider an automatic and effective numerical method for the determination of the constraint function $\beta(\mathbf{x}, t)$:

1. Set β as a constant:

$$\beta(\mathbf{x}, 0) = \beta_0. \qquad (29)$$

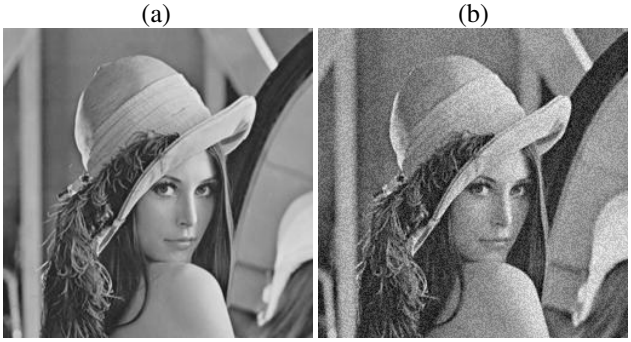

Fig. 1. Lenna: (a) The original image g and (b) a noisy image f with Gaussian noise (PSNR: 24.8)

2. For $n = 2, 3, \cdots$

(2a) Compute the absolute residual and a quantity G_{Res}^{n-1}:

$$\begin{aligned}
R^{n-1} &= |f - u^{n-1}|, \\
G_{Res}^{n-1} &= \max\left(0,\, \mathcal{S}_m(R^{n-1}) - \overline{R^{n-1}}\right), \qquad (30)
\end{aligned}$$

where $\mathcal{S}_m$ is a smoothing operator and $\overline{R^{n-1}}$ denotes the L^2-average of R^{n-1}.

(2b) Update:

$$\beta^n = \beta^{n-1} + \gamma^n\, G_{Res}^{n-1}, \qquad (31)$$

where γ^n is a scaling factor having the property: $\gamma^n \to 0$ as $n \to \infty$.

The above procedure, Eqs. (29)-(31), is called the *texture-free residual* (TFR) parameterization. See [9] for more details.

In practice, one may wish to limit the parameter in a prescribed interval, i.e., $\beta(\mathbf{x}, t) \in [\beta_0,\, \beta_1]$. Also one may want to update the parameter a few times only. Thus we can update the TFR parameter β in the first few iterations, say, four. In the case, the scaling factor γ^n can be selected as follows:

$$\gamma^n\, \|G_{res}^{n-1}\|_\infty = \eta\, (\beta_1 - \beta_0), \quad \eta = \begin{cases} 0.4, & n = 2, \\ 0.3, & n = 3, \\ 0.2, & n = 4, \\ 0.1, & n = 5. \end{cases} \qquad (32)$$

4. NUMERICAL EXPERIMENTS

This section reports some numerical examples to show the effectiveness of using a new non-standard anisotropic diffusion model incorporating the TFR parametrization. We compare the performance of conventional ITV model and ITV model with TFR parametrization (ITV-TFR), with our new non-standard anisotropic diffusion model with TFR parametrization (NSAD-TFR).

For the examples in this section, images are first scaled to have values in [0,1] and after denoising, it is scaled back

Fig. 2. Lenna: Restored images u by using (a) ITV, (b) ITV-TFR, and (c) NSAD-TFR model

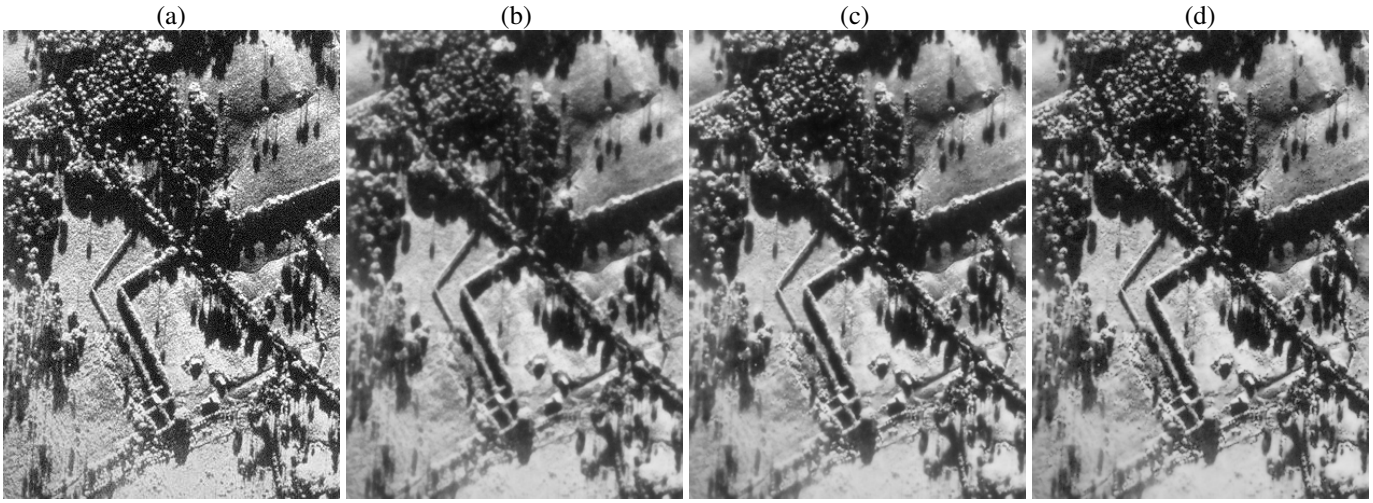

Fig. 3. Cuba: (a) The original image g, restored images u by using (b) ITV, (c) ITV-TFR, and (d) NSAD-TFR model

for the 8-bit display. We set the parameters $\epsilon = 0.05,\ \beta_0 = 0.5,\ \beta_1 = 5.0$, and $\Delta t = 1$. The constant β for ITV model is set to 0.6. Choose $C = 3$ and $\alpha = 1$ for our new model Eq. (12). We define a peak signal-to-noise ratio (PSNR) as follows:

$$\text{PSNR} \equiv 10 \log_{10} \left(\frac{\sum_{ij} 255^2}{\sum_{ij} (g_{ij} - u_{ij})^2} \right) \text{dB}, \qquad (33)$$

where g denotes the original clear image and u is the processed image. Note that PSNR value increases as the l^2 error of processed image u decreases.

The three models are used for noise removal of a Lenna image when the original image (Figure 1(a)) is contaminated by a Gaussian noise of PSNR=24.8 (Figure 1(b)). In Figure 2, restored image u by using the ITV model (Figure 2(a)), ITV-TFR model (Figure 2(b)), and NSAD-TFR model (Figure 2(c)) are presented. It can be easily seen from Figure 2(a) that the ITV model introduces a large amount of nonphysical dissipation and it makes the image blurry (PSNR=28.5). The restored image using the ITV-TFR model in Figure 2(b) show much less nonphysical dissipation (PSNR=30.2). The use of NSAD-TFR model in Figure 2(c) produces the best restored image (PSNR=30.5). It keeps most fine structures of the original image. Especially, the restored image keeps details on the feather of the hat better than other two models. Here the ITV model took 3 iterations, ITV-TFR model took 6 iterations, and NSAD-TFR model took 15 iterations to obtain the results seen in Figure 2. The optimal number of iterations is chosen to restore the best image, measured in PSNR and visual verification. This example indicates that our new NSAD-TFR model also works better than the conventional models for images without having speckle noise.

The original aerial photograph taken of Cuba during the missile crisis is shown in Figure 3(a). This original SAR image was obtained from the Central Intelligence Agency (CIA) website [7]. As one can see from Figure 3(a), the original image itself contains lots of speckle type noise. Therefore, the three models are applied directly to the original image for denoising without applying any artificial noise. The restored image in Figure 3(b) using the conventional ITV model removes most speckle noise presented in the original image but too much nonphysical dissipation induces the loss of fine

structure in the image. For ITV model, the restoration took 3 iterations. Figure 3(c) using the ITV-TFR model presents better restored image than the ITV model. However, the restored image still suffers from the noticeable amount of dissipation. Here for the ITV-TFR model, the best restored image was obtained after 6 iterations. Figure 3(d) shows that the new model removes noise satisfactorily while it keeps the fine structure of the image. The details of trees and buildings, etc. are very well preserved. The image in Figure 3(d) was obtained after 12 iterations. Note that the original image itself is not clear on the lower left corner which results in the blurriness of all three denoised images in that region. However, the NSAD-TFR model still has the best result among the three restored images.

5. CONCLUSIONS

PDE-based models, especially TV-based models can answer fundamental questions arising in image restoration better than other models. However, their minimizing energy functionals are derived based on the additive Gaussian noise which is inappropriate for speckle noise removal since speckle noise is often assumed to be multiplicative. Moreover, TV-based models produce nonphysical dissipation and consequently lose fine structures in the image during the denoising process. In this article, a new physics based non-standard anisotropic diffusion model incorporating with TFR parametrization (NSAD-TFR), has been introduced for an efficient noise removel for images having speckle noise. The new NSAD-TFR model controls the speed of dissipation by using the new coefficient of anisotropic diffusion in the conventional ITV model. A new numerical procedure for the NSAD model has been proved to be mathematically stable and satisfy the maximum principle. It has been verified from numerical examples that the new model with stable numerical procedure better preserves fine structures while removing speckle noise more satisfactorily than the ITV model and ITV model with TFR parametrization.

6. REFERENCES

[1] L. Alvarez, P. Lions, and M. Morel, "Image selective smoothing and edge detection by nonlinear diffusion. II," *SIAM J. Numer. Anal.*, vol. 29, pp. 845–866, 1992.

[2] F. Catte, P. Lions, M. Morel, and T. Coll, "Image selective smoothing and edge detection by nonlinear diffusion." *SIAM J. Numer. Anal.*, vol. 29, pp. 182–193, 1992.

[3] Y. Cha and S. Kim, "MONTE: The method of nonflat time evolution in PDE-based image restoration," (submitted).

[4] T. Chan, S. Osher, and J. Shen, "The digital TV filter and nonlinear denoising," Department of Mathematics, University of California, Los Angeles, CA 90095-1555, Technical Report #99-34, October 1999.

[5] J. Douglas, Jr. and J. Gunn, "A general formulation of alternating direction methods Part I. Parabolic and hyperbolic problems," *Numer. Math.*, vol. 6, pp. 428–453, 1964.

[6] J. Douglas, Jr. and S. Kim, "Improved accuracy for locally one-dimensional methods for parabolic equations," *Mathematical Models and Methods in Applied Sciences*, vol. 11, pp. 1563–1579, 2001.

[7] J. H. Hansen, "Learning from the Past: Soviet Deception in the Cuban Missile Crisis," *Studies in Intelligence: Journal of American Intelligence Professional*, vol. 46, no.1, 2002, Central Intelligence Agency, `www.odci.gov/csi/studies/vol46no1/article06.html`

[8] S. Kim, "PDE-based image restoration: A hybrid model and color image denoising," *IEEE Trans. Image Process.*, vol. 15, no.5, pp. 1163–1170, 2006.

[9] S. Kim and H. Lim, "Non-convex PDE-based minimization for simultaneous image denoising and edge enhancement," (accepted to Electron. J. Differ. Equ.).

[10] K. Krissian, R. Kikinis, C. F. Westin, and K. Vosburgh, "Speckle-constrained filtering of ultrasound images" *IEEE Computer Vision and Pattern Recognition*, 2005, pp.II:547–552.

[11] K. Krissian, K. Vosburgh, R. Kikinis, and C. F. Westin, "Anisotropic diffusion of ultrasound constrained by speckle noise model" Laboratory of Mathematics in Imaging, Harvard Medical School, Brigham and Women's Hospital, Department of Radiology, 75 Francis Street, 02115 Boston, MA, Technical report, 2004.

[12] A. Marquina and S. Osher, "Explicit algorithms for a new time dependent model based on level set motion for nonlinear deblurring and noise removal," *SIAM J. Sci. Comput.*, vol. 22, pp. 387–405, 2000.

[13] M. Nitzberg and T. Shiota, "Nonlinear image filtering with edge and corner enhancement," *IEEE Trans. on Pattern Anal. Mach. Intell.*, vol. 14, pp. 826–833, 1992.

[14] P. Perona and J. Malik, "Scale-space and edge detection using anisotropic diffusion," *IEEE Trans. on Pattern Anal. Mach. Intell.*, vol. 12, pp. 629–639, 1990.

[15] L. Rudin, S. Osher, and E. Fatemi, "Nonlinear total variation based noise removal algorithms," *Physica D*, vol. 60, pp. 259–268, 1992.

[16] J. Russ, *The image processing handbook*. CRC Press, Inc., Bocal Raton, Florida, 1992.

[17] Y. You, W. Xu, A. Tannenbaum, and M. Kaveh, "Behavioral analysis of anisotropic diffusion in image processing," *IEEE Trans. Image Process.*, vol. 5, pp. 1539–1553, 1996.